

Active Brownian particles in external force fields: Field-theoretical models, generalized barometric law, and programmable density patterns

Jens Bickmann ^{*}, Stephan Bröker ^{*}, Michael te Vrugt , and Raphael Wittkowski [†]

Institut für Theoretische Physik, Center for Soft Nanoscience, Westfälische Wilhelms-Universität Münster, 48149 Münster, Germany



(Received 31 July 2023; accepted 24 August 2023; published 9 October 2023)

We investigate the influence of external forces on the collective dynamics of interacting active Brownian particles in two as well as three spatial dimensions. Via explicit coarse graining, we derive predictive models, i.e., models that give a direct relation between the models' coefficients and the bare parameters of the system, that are applicable for space- and time-dependent external force fields. We study these models for the cases of gravity and harmonic traps. In particular, we derive a generalized barometric formula for interacting active Brownian particles under gravity that is valid for low to high concentrations and activities of the particles. Furthermore, we show that one can use an external harmonic trap to induce motility-induced phase separation in systems that, without external fields, remain in a homogeneous state. This finding makes it possible to realize programmable density patterns in systems of active Brownian particles. Our analytic predictions are found to be in very good agreement with Brownian dynamics simulations.

DOI: [10.1103/PhysRevE.108.044601](https://doi.org/10.1103/PhysRevE.108.044601)

I. INTRODUCTION

Active Brownian particles (ABPs) are particles that undergo Brownian motion together with constant self-propulsion [1–4]. Under the influence of external fields, they can show a variety of effects [4–6]. This includes anomalous sedimentation profiles under gravity [7–9], self-induced polar ordering [10–15], trapping [15–17], superfluidity [18,19], effective diffusion coefficients [7,11,20–23], and self-organized fluid pumps [24]. In addition, ABPs show an accumulation at repulsive walls or interfaces [25,26]. Such walls or interfaces can be described via an external force field [27]. A force field can also be used to determine properties like pressure in far-from-equilibrium systems [14,28,29]. Furthermore, the nonequilibrium dynamics of active particles in external fields is very important for future applications of such particles in medicine and materials science, where active particles can, e.g., perform drug delivery [30–34] and form active materials with exceptional properties [35], respectively. It has been demonstrated that the control over the particles that is needed for such applications can be well achieved via external fields [34,36]. The active agents can be either artificial self-propelled microparticles [37–42] or motile microorganisms [43–45]. Both are frequently and successfully described as ABPs, including even run-and-tumble particles like *Escherichia coli* bacteria [45–48].

Despite the importance of the behavior of ABPs under an external force, there exist only a few, and often very specific, theoretical models for the nonequilibrium dynamics of ABPs in external force fields. Sedimentation profiles for noninteracting ABPs in two and three spatial dimensions are derived in Ref. [14] and further compared with experimental data.

The authors of this work found a qualitative agreement with the traditional barometric formula only after a certain height. In Ref. [9], a coarse graining in Fourier space with long-wavelength approximations was used to obtain a model for noninteracting ABPs under gravity in three spatial dimensions and in the presence of a confining wall, resulting in a refined barometric formula in the steady-state limit. By neglecting translational diffusion, the steady-state equation for systems of noninteracting ABPs in two spatial dimensions under the effect of various external forces was solved analytically in Ref. [49]. Reference [23] is even able to present an exact result for the steady state in systems of noninteracting ABPs in two dimensions under gravity and with translational diffusion, but considers only situations with fixed polarization of the particle orientations. Another work [15] investigates “L”-shaped particles and their polar ordering in gravitational fields based on theory and experiments, but their method does not include a field-theoretical description. ABPs confined by two-dimensional optical traps are investigated in Ref. [17], where a corresponding dynamical density functional theory (DDFT) [50] for interacting ABPs, based on a mapping to passive colloidal particles, was derived. Further work on DDFT for microswimmers in confinement can be found in Refs. [51–53]. The DDFT approach, however, has the consequence that the model is only valid at low densities and low activities of the particles. In Ref. [54] a statistical field theory for a specific model system with arbitrary external forces was derived using the unified colored-noise approximation [55].

A drawback of these approaches is that the corresponding equations are either nonlocal, which makes them very difficult to solve, or nonpredictive. A *predictive theory*, in our terminology, is a theory that includes explicit expressions for all coefficients of the model and that therefore, once the microscopic description is fixed, in principle does not contain free parameters. Such a theory may contain approximations, and how accurate it is depends on how good these

^{*}These authors contributed equally to this work.

[†]Corresponding author: raphael.wittkowski@uni-muenster.de

approximations are. The validity of many existing active field theories that include external fields (such as active DDFT) is relatively limited in the far-from-equilibrium regime. A local predictive field theory that considers arbitrary external force fields, while still accounting for the full interaction between the particles, is still missing and would be an important asset for this area of research. Such a theory can be derived using the interaction-expansion method [56,57], which is based on the Bogoliubov-Born-Green-Kirkwood-Yvon (BBGKY) hierarchy.

In this article we derive such a local predictive field theory for interacting ABPs in two and three spatial dimensions under the influence of external force fields that can be space and time dependent. As results, we present models that describe the dynamics of the particles up to the second and fourth order in derivatives. We show that in the case of the second-order-derivatives model, external forces mimic advection. Using our models we study the stationary states of the particle dynamics for the case of two common types of external fields: gravity and harmonic traps. For the case of gravity, we observe deviations from the barometric density law due to an interplay of the particle activity and interactions. For harmonic traps, we show that the ABPs can be induced to undergo motility-induced phase separation (MIPS) [58] at desired locations. We verify this result by comparing with Brownian dynamics simulations. Our analytical predictions and the simulation data are found to be in very good agreement.

This article is structured as follows: In Sec. II, we derive the models and describe the simulation setup. We apply our model to the cases of gravity fields and harmonic traps and discuss the results in Sec. III. Finally, we conclude in Sec. IV.

II. METHODS

A. Theoretical model

To derive a local predictive field theory for interacting ABPs in external force fields, we consider systems of N spherical ABPs in two (2D) and three (3D) spatial dimensions. The i th ABP is described using its center-of-mass position $\vec{r}_i(t)$ and normalized orientation vector $\hat{u}_i(t)$, which are functions of time t . Its motion is influenced by an external force field $\vec{F}_{\text{ext}}(\vec{r}_i, t)$ that can depend on the particle position and time. The translational motion of the ABPs considered here is given by the Langevin equation

$$\dot{\vec{r}}_i(t) = \vec{\xi}_{T,i} + v_0 \hat{u}_i + \beta D_T \vec{F}_{\text{int},i}(\{\vec{r}_i\}) + \vec{v}_{\text{ext}}(\vec{r}_i, t), \quad (1)$$

which holds for 2D and 3D. A partial derivative with respect to time is denoted by an overdot. For the rotational motion of the ABPs, we use the Langevin equations

$$\dot{\phi}_i = \xi_{R,i} \quad \text{for 2D}, \quad (2)$$

$$\dot{\hat{u}}_i = \hat{u}_i \times \vec{\xi}_{R,i} \quad \text{for 3D}, \quad (3)$$

with the parametrization

$$\hat{u}_i(\phi) = (\cos(\phi), \sin(\phi))^T \quad \text{for 2D}, \quad (4)$$

$$\hat{u}_i(\theta, \phi) = (\cos(\phi) \sin(\theta), \sin(\phi) \sin(\theta), \cos(\theta))^T \quad \text{for 3D} \quad (5)$$

of the orientation vector by polar (2D) and spherical (3D) coordinates, respectively. In Eqs. (1)–(3), the translational and rotational Brownian motion of the i th particle is described by statistically independent Gaussian white noises $\vec{\xi}_{T,i}(t)$ for translation (2D and 3D) and $\xi_{R,i}(t)$ (2D) or $\vec{\xi}_{R,i}(t)$ (3D) for rotation, respectively. These noises have zero mean, and their correlations are given by $\langle \vec{\xi}_{T,i}(t_1) \otimes \vec{\xi}_{T,j}(t_2) \rangle = 2D_T \delta_{ij} \mathbb{1}_n \delta(t_1 - t_2)$ for translation (2D and 3D) and $\langle \xi_{R,i}(t_1) \xi_{R,j}(t_2) \rangle = 2D_R \delta_{ij} \delta(t_1 - t_2)$ (2D) or $\langle \vec{\xi}_{R,i}(t_1) \otimes \vec{\xi}_{R,j}(t_2) \rangle = 2D_R \delta_{ij} \mathbb{1}_3 \delta(t_1 - t_2)$ (3D) for rotation with the ensemble average $\langle \cdot \rangle$, dyadic product \otimes , translational and rotational diffusion coefficients D_T and D_R , respectively, Kronecker delta δ_{ij} , and the n -dimensional identity matrix $\mathbb{1}_n$, where $n = 2$ for 2D and $n = 3$ for 3D. For the spherical particles, the Stokes-Einstein-Debye relation $D_R = 3D_T/\sigma^2$ holds, where σ is their diameter. Furthermore, v_0 denotes the propulsion speed of an individual ABP that is not affected by interactions or an external force, $\beta = 1/(k_B T)$ is the thermodynamic beta with Boltzmann constant k_B and absolute temperature T , and $\vec{F}_{\text{int},i}(\{\vec{r}_i\}) = -\sum_{j=1, j \neq i}^N \vec{\nabla}_{\vec{r}_i} U_2(\|\vec{r}_i - \vec{r}_j\|)$ is the particle-particle interaction force, where $\vec{\nabla}_{\vec{r}_i}$ denotes the del operator with respect to \vec{r}_i and U_2 the pair-interaction potential of the particles. The propulsion speed that would solely originate from the external force can be written as $\vec{v}_{\text{ext}}(\vec{r}_i, t) = \beta D_T \vec{F}_{\text{ext}}(\vec{r}_i, t)$ and constitutes the central object of our investigation.

Equations (1)–(3) correspond to the statistically equivalent Smoluchowski equation

$$\dot{\mathfrak{P}} = \sum_{i=1}^N \left(-v_0 \hat{u}_i \cdot \vec{\nabla}_{\vec{r}_i} \mathfrak{P} + (D_T \Delta_{\vec{r}_i} + D_R \mathfrak{R}_i^2) \mathfrak{P} - \vec{\nabla}_{\vec{r}_i} \cdot ([\beta D_T \vec{F}_{\text{int},i}(\{\vec{r}_i\}) + \vec{v}_{\text{ext}}(\vec{r}_i, t)] \mathfrak{P}) \right), \quad (6)$$

which describes the time evolution of the many-particle probability density $\mathfrak{P}(\{\vec{r}_i\}, \{\hat{u}_i\}, t)$ that depends on the whole set of position vectors $\{\vec{r}_i\}$, the set of orientations $\{\hat{u}_i\}$, and time t . Here, the Laplace operator acting on the i th particle is denoted as $\Delta_{\vec{r}_i} \equiv \vec{\nabla}_{\vec{r}_i}^2$, and the rotational operator is given by $\mathfrak{R}_i = \frac{\partial}{\partial \phi_i}$ (2D) or $\mathfrak{R}_i = \hat{u}_i \times \frac{\partial}{\partial \hat{u}_i}$ (3D).

The further derivation of a field-theoretical model is based on the *interaction-expansion method* [56,59–62], which is explained in Appendix A and reviewed in Ref. [57]. By integrating over all degrees of freedom except for those of one particle, renaming the remaining degrees of freedom as \vec{r} and \hat{u} , and multiplying with N , an equation for the one-particle density field,

$$\varrho(\vec{r}, \phi, t) = N \left(\prod_{\substack{j=1 \\ j \neq i}}^N \int_{\mathbb{R}^2} d^2 r_j \int_0^{2\pi} d\phi_j \right) \mathfrak{P} \Big|_{\substack{\vec{r}_i = \vec{r}, \\ \phi_i = \phi}} \quad \text{for 2D}, \quad (7)$$

$$\varrho(\vec{r}, \hat{u}, t) = N \left(\prod_{\substack{j=1 \\ j \neq i}}^N \int_{\mathbb{R}^3} d^3 r_j \int_{\mathbb{S}} d^2 u_j \right) \mathfrak{P} \Big|_{\substack{\vec{r}_i = \vec{r}, \\ \hat{u}_i = \hat{u}}} \quad \text{for 3D}, \quad (8)$$

can be obtained. We denote the surface of the unit sphere in 3D by \mathbb{S} .

Additional steps of the derivation include a Fourier expansion (2D) [56] or spherical harmonics expansion (3D) [60]

of the particle pair-distribution function g , a gradient expansion [63–65] of integrals that contain the interaction force, an orientational expansion of ϱ into Cartesian order-parameter tensors [66], and a quasistationary approximation (QSA) [56,59,60] of the resulting coupled equations for the Cartesian order-parameter fields.

The pair-distribution function g relates the two-particle density $\varrho^{(2)}(\vec{r}, \vec{r}', \hat{u}, \hat{u}', t)$ to one-particle densities $\varrho(\vec{r}, \hat{u}, t)$:

$$\varrho^{(2)}(\vec{r}, \vec{r}', \hat{u}, \hat{u}', t) = g(\vec{r}, \vec{r}', \hat{u}, \hat{u}', t) \varrho(\vec{r}, \hat{u}, t) \varrho(\vec{r}', \hat{u}', t). \quad (9)$$

Both correlation functions depend on the number of spatial dimensions and are in general unknown. However, for stationary states, where g has translational and rotational invariance and is time independent, analytic representations of g exist in 2D [67] and 3D [68]. To apply these representations, we assume that g is approximately translationally and rotationally invariant and time independent on the scale of the particle interaction length and angular relaxation time. For short-range interactions and weak spatial and temporal changes of the external force, these assumptions are well justified.

After performing the aforementioned derivation steps, the dynamics of the system is described in terms of the local particle-number density,

$$\rho(\vec{r}, t) = \int_0^{2\pi} d\phi \varrho(\vec{r}, \hat{u}(\phi), t) \quad \text{for 2D}, \quad (10)$$

$$\rho(\vec{r}, t) = \int_{\mathbb{S}} d^2u \varrho(\vec{r}, \hat{u}, t) \quad \text{for 3D}. \quad (11)$$

We restrict the gradient expansion to terms of maximal order 2 in derivatives and, since we want to consider weak external fields, we neglect terms of second or higher order in \vec{v}_{ext} . The resulting model is an advection-diffusion equation,

$$\dot{\rho} = \vec{\nabla} \cdot [-\vec{v}_{\text{ext}}\rho + D(\rho)\vec{\nabla}\rho], \quad (12)$$

with density-dependent diffusion coefficient,

$$D(\rho) = D_T + a_0 + a_1\rho + a_2\rho^2. \quad (13)$$

In Eq. (12), the external force field mimics an advection velocity, and the coefficients $\{a_i\}$ in Eq. (13) depend on the number of spatial dimensions of the system. These coefficients are related to microscopic parameters of the system by equations that are given in Appendix B. In the limit of dilute suspensions, the density dependence of $D(\rho)$ can be neglected and Eq. (12) obtains the same form as for passive particles but with a different diffusion coefficient $D_T + a_0$. This provides a mapping of the ABPs to passive particles with an effective diffusion coefficient [20]. When ignoring the advection term $-\vec{\nabla} \cdot (\vec{v}_{\text{ext}}\rho)$, Eq. (12) becomes equivalent to Eqs. (20)–(22) in Ref. [56] for 2D or Eqs. (21)–(23) in Ref. [60] for 3D. Equation (12) constitutes the simplest model describing systems of ABPs under the influence of an external force.

Although this second-order-derivatives model can predict the onset of MIPS, one might be interested also in a description of the further time evolution of MIPS. For such a description, one needs at least four orders in derivatives, as they are present in models like Active Model B [69], Active Model B + [70], and predictive field theories proposed in

Refs. [56] (2D) and [60] (3D). By truncating the gradient expansion at fourth order in derivatives and performing a QSA, we obtain a field theory that extends the phase-field models of Refs. [56,60] towards an external force field. The dynamic equation for the density field in this field theory is

$$\dot{\rho} = -\vec{\nabla} \cdot (\vec{J}^{(\text{int})} + \vec{J}^{(\text{ext})}). \quad (14)$$

Here, $\vec{J}^{(\text{int})}$ denotes the density current of ABPs under no external force, which is given by Eq. (25) in Ref. [56] for 2D and Eq. (26) in Ref. [60] for 3D and can also be found in the Supplemental Material [71]. The current $\vec{J}^{(\text{ext})}$ arises from the external force field. When we again neglect terms of second or higher order in \vec{v}_{ext} , the current $\vec{J}^{(\text{ext})}$ reads

$$\begin{aligned} \vec{J}^{(\text{ext})} = & \vec{v}_{\text{ext}}\rho + (b_1 + b_2\rho + b_3\rho^2)\vec{\nabla} \cdot (\vec{v}_{\text{ext}} \otimes \vec{\nabla}\rho) \\ & + (b_4 + b_3\rho)(\vec{v}_{\text{ext}} \cdot \vec{\nabla}\rho)\vec{\nabla}\rho, \end{aligned} \quad (15)$$

where we use the notation $\vec{a} \cdot (\vec{b} \otimes \vec{c}) = (\vec{a} \cdot \vec{b})\vec{c}$. Microscopic expressions for the coefficients $\{b_i\}$ are given in Appendix B.

Note that the advection-diffusion model (12) and the extended phase-field model (14) of ABPs in external fields can be applied for low to high particle densities and small to large activities. These models constitute the first main result of this article. In the second-order-derivatives model (12), the external force field enters only via the “standard” term $-\vec{\nabla} \cdot (\vec{v}_{\text{ext}}\rho)$ that is known also from other theories [50]. However, in the fourth-order-derivatives model, the external force field \vec{v}_{ext} enters in several nontrivial terms that are not familiar from passive theories. These terms arise from the coupling of the external force field to the polarization field that describes the orientation of the particles.

If one considers stationary states, it follows from Eq. (12) that the density field must obey the equation

$$D(\rho)\vec{\nabla}\rho = \vec{v}_{\text{ext}}\rho. \quad (16)$$

Note that \vec{v}_{ext} can still be time dependent, albeit only on the timescale of the relaxation time of the stationary state or slower. Equation (16) allows stationary-state solutions for the density of interacting ABPs to be obtained in a simple way. It is an extension of the equation $D(\rho) = 0$ for the stationary state of interacting ABPs in the absence of external forces [72].

B. Simulations

In our simulations, we focus on the 2D case to keep the computational effort moderate. Numerical solutions of the stationary-state equation (16) are obtained using the adaptive Runge-Kutta-Fehlberg 4(5) method with an accuracy goal of 10^{-10} [73].

When studying harmonic traps, we perform also Brownian dynamics simulations based on the Langevin equations (1) and (2) using a modified version of the software package LAMMPS [74]. As interaction potential, we choose the purely repulsive Weeks-Chandler-Andersen potential [75],

$$U_2(r) = \begin{cases} 4\varepsilon\left(\left(\frac{\sigma}{r}\right)^{12} - \left(\frac{\sigma}{r}\right)^6\right) + \varepsilon, & \text{if } r \leq 2^{1/6}\sigma, \\ 0, & \text{else} \end{cases} \quad (17)$$

with the interaction energy ε and particle diameter σ . To incorporate a circular harmonic trap, we prescribe the local change of the particle velocity due to the trapping force as

$$\vec{v}_{\text{ext}}(\vec{r}, t) = \begin{cases} -k(\vec{r} - \vec{r}_c), & \text{if } \|\vec{r} - \vec{r}_c\| < r_t, \\ 0, & \text{else} \end{cases} \quad (18)$$

with the parameter k determining the trapping strength, the center of the trap \vec{r}_c being in the center of our simulation domain, and the radius of the trap r_t . We varied $kr_t/v_0 \in [0, 1]$ and $r_t/\sigma \in [0, 24]$ and used a quadratic simulation domain with edge length 256σ and periodic boundary conditions. The initial particle distribution is uniform and random with overall packing density $\Phi = \pi\bar{\rho}\sigma^2/4 = 0.2$, where $\bar{\rho}$ is the spatially averaged particle-number density, resulting in $\approx 17\,000$ particles in the system. Since the simulation domain is much larger than the largest trap considered in this work and since the particle packing density is moderate, the particle density outside the trap does not change for more than $\approx 10\%$, even if so many particles are trapped that the largest trap is closely packed with particles. We use Lennard-Jones units and choose the particle diameter σ , Lennard-Jones time $\tau_{\text{LJ}} = \sigma^2/(\beta D_T \varepsilon)$, and interaction energy ε as units of length, time, and energy, respectively. We describe the activity of the particles by the dimensionless Péclet number $\text{Pe} = v_0\sigma/D_T$, for which we choose $\text{Pe} = 100$ in all simulations. In addition, we choose $v_0 = 24\sigma/\tau_{\text{LJ}}$ to be consistent with previous works [59,61,67,76–79]. The Langevin equations (1) and (2) are solved for a total simulation time of $1500\tau_{\text{LJ}}$ in the simulations that correspond to the case of a gravitational external force, with a time-step size of $2 \times 10^{-5}\tau_{\text{LJ}}$ and $1 \times 10^{-4}\tau_{\text{LJ}}$ for the cases with and without interaction, respectively, and, for a total simulation time of $2000\tau_{\text{LJ}}$ in the simulations that consider harmonic traps, with a time-step size of $5 \times 10^{-5}\tau_{\text{LJ}}$. To examine the density distribution under the influence of gravity, we started with 10 000 randomly distributed particles and discarded the first $500\tau_{\text{LJ}}$ to allow for sufficient relaxation of the system. For each value of v_g , five different simulations were performed, and the density at each height was extracted every τ_{LJ} . We evaluate the collective dynamics of the ABPs by calculating the mean particle density ρ_{trap} inside a trap. To ensure reliable and robust results, we measure after an initial simulation period of $1600\tau_{\text{LJ}}$ the interaction energy per particle ten times with a period of $40\tau_{\text{LJ}}$ between each measurement and average over the individual measurements.

For some simulations, where strong traps were considered, the time-step size was halved. When passive particles, which move slowly, are combined with large and strong traps, which collect many particles until they are filled, the simulation time and the period between measurements were doubled. An overview about the different simulations and their time-step sizes, simulation times, and periods between measurements is provided in Ref. [80].

III. RESULTS

We consider two different external force fields: gravity and harmonic traps. All presented results are obtained for 2D and an activity of $\text{Pe} = 100$.

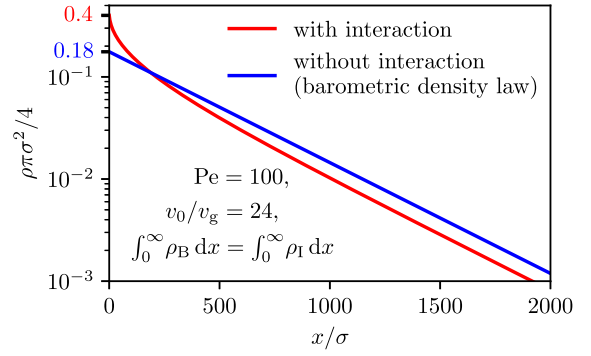


FIG. 1. Numerical solution of Eq. (19) for interacting ABPs under gravity (red) and barometric density law (20) for noninteracting ABPs under gravity (blue) for $v_g/v_0 = 1/24$. We have chosen $\rho_I(0)\pi\sigma^2/4 = 0.4$ for the curve representing the interacting particles. The two functions are normalized so that the total number of particles of the system is the same for both cases. This leads to $\rho_B(0)\pi\sigma^2/4 = \rho_{B,0}\pi\sigma^2/4 \approx 0.18$. See Ref. [80] for the raw data corresponding to this figure.

A. Gravity

In the presence of gravity, the external-force contribution to the particle velocity reads $\vec{v}_{\text{ext}} = -v_g\vec{e}_x$, where v_g is the sedimentation speed caused by the gravitational field and \vec{e}_x is the unit vector in x direction. Equation (16) now reduces to the one-dimensional differential equation

$$D(\rho)\frac{\partial}{\partial x}\rho = -v_g\rho. \quad (19)$$

In the dilute limit, where $D(\rho) \rightarrow D_T + a_0$, this equation is solved by the barometric density law

$$\rho_B(x) = \rho_{B,0}e^{-\frac{v_g x}{D_T + a_0}} \quad (20)$$

with $\rho_{B,0} = \rho_B(0)$. Here $D_T + a_0$ is the effective diffusion coefficient of the ABPs that corresponds to an effective temperature $T_{\text{eff}} = (D_T + a_0)\gamma/k_B = T[1 + v_0^2\tau_{\text{LJ}}^2/(6\sigma^2)]$ of the system, where $\gamma = k_B T/D_T$ denotes the translational friction coefficient of a particle. For noninteracting particle systems, Eq. (20) is an exact steady-state solution of the second-order-derivatives model (19). Since the coefficient a_0 is non-negative, Eq. (20) suggests that in a gravitational field the density of ABPs decreases slower for increasing x than the density of passive Brownian particles at the same temperature T . Note that not the physical temperature T of the solvent surrounding the particles but the effective temperature T_{eff} that can be associated with the particle motion [20] describes the slope of the exponential decay.

For interacting particles, one needs to solve Eq. (19) numerically, since $D(\rho)$, given by Eq. (13), is now density dependent. Obtaining the corresponding numerical solution $\rho_I(x)$, however, requires knowledge of the values of the coefficients $\{a_i\}$ and of the velocity v_g . To determine the values of $\{a_i\}$ for the considered ABPs, we use Eqs. (B1) and (B3) and Eqs. (B8) and (B10) from Appendix B.

The results, obtained for $v_g/v_0 = 1/24$, are shown in Fig. 1. We see small deviations between the curves for interacting and noninteracting ABPs for small values of x , i.e., in the high-density regime where the density dependence of

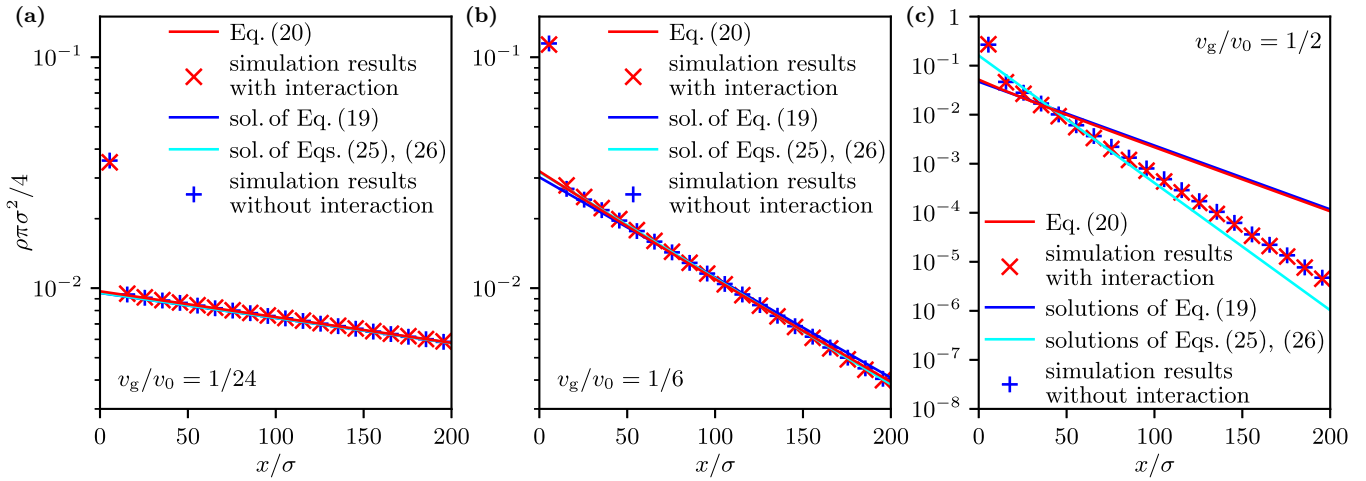


FIG. 2. Numerical solution of Eq. (19) for interacting ABPs under gravity (red), barometric density law (20) for noninteracting ABPs under gravity (dark blue), and solution of Eqs. (25) and (26) for noninteracting ABPs (light blue) for (a) $v_g/v_0 = 1/24$, (b) $v_g/v_0 = 1/6$, and (c) $v_g/v_0 = 1/2$ compared to density obtained from Brownian dynamics simulations for interacting (blue crosses) and noninteracting (red crosses) ABPs. The particles in the simulation accumulate at the wall, resulting in a higher density at $x/\sigma \approx 0$. Particle interactions do not have a significant effect on the overall distribution. The theoretical prediction (20) and the numerical data are in very good agreement for $v_g/v_0 \ll 1$ and become increasingly inaccurate for larger values of v_g/v_0 . In contrast, the theoretical prediction from Eqs. (25) and (26) is in good agreement with the simulation results even for stronger gravitational fields. We have chosen the initial values for Eqs. (19) and (20) to match the number of particles in the simulation while excluding the particles at low values of x ($x/\sigma \leq 10.5$, which corresponds to excluding the first bin) to account for the accumulation at the wall which the theory cannot include. The solution of Eqs. (25) and (26) has been approximated as explained in the text, with the one remaining initial condition used as a fit parameter. See Ref. [80] for the raw data corresponding to this figure.

$D(\rho)$ is important: The curve that considers interactions does not follow the barometric density law. With interactions the density of the ABPs is larger than without interactions in this regime. This originates from the fact that the activity creates an effective attractive interaction potential [81] that replaces the purely repulsive interaction of the particles [54] and leads to accumulation where interactions are relevant. However, this effect is rather weak in our simulations, as the density is quite low even for small values of x . The effective attractive interaction enters Eq. (19) through the coefficients a_1 and a_2 in the density-dependent diffusion coefficient (13) and their contributions increase with ρ . For large values of v_0 , as they are considered here, the contribution of the coefficient a_1 reduces the value of $D(\rho)$, which leads to the observed accumulation of ABPs. Interestingly, our analytic approach reveals that this mechanism is the same as that leading to MIPS for even larger densities. To see this one has to take into account that the coefficient a_1 determines also the density dependence of the mean swimming speed of ABPs [56,60] and that a sufficiently strong decrease of the mean swimming speed with increasing density leads to MIPS [58]. For large values of x , i.e., in the low-density regime, both curves show the same qualitative behavior, since interactions between particles are rare in this regime. The curves now follow an exponential decay with the same decay constant $-v_g/(D_T + a_0)$. Due to particle-number conservation, however, the density of interacting ABPs is smaller than the density of noninteracting ABPs for large values of x .

What still needs to be investigated, however, is whether the barometric density law also holds for stronger gravitational fields and whether it agrees with simulation results.

Therefore, in addition to $v_g = v_0/24$, we also investigated the cases $v_g = v_0/6$ and $v_g = v_0/2$. Moreover, we ran particle-resolved computer simulations on a domain that is open in the positive x direction and has a wall at the bottom edge ($x = 0$). For the y direction, a width of 2048σ and periodic boundary conditions were chosen. (Due to the symmetry of the system in the direction orthogonal to \vec{v}_{ext} , we can compare a one-dimensional theory with two-dimensional simulations here.) Active particles accumulate at walls, especially if (as is the case here) the external force pushes them there [82–84]. The wall is, however, not present in our theory. Hence the theory cannot account for the accumulation effect close to it. Therefore we chose the initial conditions when solving Eqs. (19) and (20) to match the total number of particles in the simulation while excluding particles at the bottom ($x/\sigma < 10.5$) to account for the accumulation at the wall.

The results are shown in Fig. 2. For all considered gravitational field strengths, there is no disagreement between simulation results with and without interactions, or between the barometric density law (20) (noninteracting case) and the numerical solution of Eq. (19) for interacting particles. What we do observe, however, is that the theoretical prediction (20) is in good agreement with the simulation results only for weak ($v_g = v_0/24$) and intermediate ($v_g = v_0/6$) external fields but ceases to be valid in the case of strong gravity ($v_g = v_0/2$).

Since interactions play a relatively small role, we can focus on the noninteracting case in our analysis of this issue. To get an improved theoretical prediction, it is worth going a step back and taking a look at how Eq. (12) is derived in the first place. (A discussion of the interacting case is found in Appendix A.) In two dimensions, integrating out Eq. (6),

using Eq. (7), and making the expansion [66,85]

$$\varrho(\vec{r}, \hat{u}, t) = \frac{1}{2\pi} (\rho(\vec{r}, t) + \vec{P}(\vec{r}, t) \cdot \hat{u} + \underline{Q}(\vec{r}, t) : \hat{u} \otimes \hat{u}) \quad (21)$$

with the concentration field $\rho(\vec{r}, t)$, the polarization vector $\vec{P}(\vec{r}, t)$, the traceless and symmetric nematic tensor $\underline{Q}(\vec{r}, t)$, and the double tensor contraction $:$ gives the exact two-field model:

$$\dot{\rho} = D_T \vec{\nabla}^2 \rho - \frac{v_0}{2} \vec{\nabla} \cdot \vec{P} - \vec{\nabla} \cdot (\vec{v}_{\text{ext}} \rho), \quad (22)$$

$$\dot{\vec{P}} = D_T \vec{\nabla}^2 \vec{P} - D_R \vec{P} - v_0 \vec{\nabla} \rho - \vec{\nabla} \cdot (\vec{v}_{\text{ext}} \otimes \vec{P}). \quad (23)$$

The nematic tensor is not relevant in the noninteracting case for the microscopic model considered here. We perform a QSA by setting $\vec{P} = \vec{0}$, giving

$$\vec{P} = \frac{D_T}{D_R} \vec{\nabla}^2 \vec{P} - \frac{v_0}{D_R} \vec{\nabla} \rho - \frac{1}{D_R} \vec{\nabla} \cdot (\vec{v}_{\text{ext}} \otimes \vec{P}). \quad (24)$$

Finally, we repeatedly insert Eq. (24) into itself, drop terms of higher than a certain order in $\vec{\nabla}$, insert the result into Eq. (22), and again drop terms of higher than a certain order in $\vec{\nabla}$. The order in gradients at which we truncate determines whether we arrive at Eq. (12), Eq. (14), or a higher-order model.

Having observed that Eq. (12) does not provide an accurate description of the ABP system for very strong gravitational fields, and further noting that the only approximation involved in the derivation of Eq. (12) in the noninteracting case is the elimination of \vec{P} , a natural next step is to find a stationary solution of the exact model given by Eqs. (22) and (23). In the stationary one-dimensional case with $v_{\text{ext}} = -v_g$, this model reduces to

$$0 = D_T \frac{\partial}{\partial x} \rho - \frac{v_0}{2} P + v_g \rho, \quad (25)$$

$$0 = D_T \frac{\partial^2}{\partial x^2} P - D_R P - v_0 \frac{\partial}{\partial x} \rho + v_g \frac{\partial}{\partial x} P. \quad (26)$$

Setting, as done in our simulations, $v_0 = 24\sigma/\tau_{\text{LJ}}$, $\text{Pe} = 100$, $D_T = v_0\sigma/\text{Pe}$, and $D_R = 3D_T/\sigma^2$, we find for $v_g/v_0 = 1/2$ the solution

$$\begin{aligned} \rho(x) = & (-0.2071005e^{-120.723x/\sigma} - 0.99287e^{-0.0597854x/\sigma} \\ & + 1.19997e^{20.7829x/\sigma})P_0 + (0.00292833e^{-120.723x/\sigma} \\ & - 0.01988115e^{-0.0597854x/\sigma} \\ & + 0.0169528e^{20.7829x/\sigma})P'_0 \\ & + (0.207028e^{-120.723x/\sigma} + 1.99049e^{-0.0597854x/\sigma} \\ & - 1.19752e^{20.7829x/\sigma})\rho_0, \end{aligned} \quad (27)$$

$$\begin{aligned} P(x) = & (0.292936e^{-120.723x/\sigma} - 0.991681e^{-0.0597854x/\sigma} \\ & + 1.69875e^{20.7829x/\sigma})P_0 + (-0.00414201e^{-120.723x/\sigma} \\ & - 0.0198574e^{-0.0597854x/\sigma} + 0.0239994e^{20.7829x/\sigma})P'_0 \\ & - (0.292833e^{-120.723x/\sigma} - 1.988115e^{-0.0597854x/\sigma} \\ & + 1.69528e^{20.7829x/\sigma})\rho_0, \end{aligned} \quad (28)$$

with $\rho_0 = \rho(0)$, $P_0 = P(0)$, and $P'_0 = P'(0)$. Imposing the condition $\lim_{x \rightarrow \infty} \rho(x) = 0$ implies that the prefactor of

$\exp(20.7829x/\sigma)$, given by $1.19997P_0 + 0.0169528P'_0 - 1.19752\rho_0$, has to vanish. Thus $\rho(x)$ is given by the sum of a term proportional to $\exp(-120.723x/\sigma)$ and a term proportional to $\exp(-0.0597854x/\sigma)$. The former is clearly negligible. Thus the theoretical model given by Eqs. (25) and (26) effectively predicts that ρ is proportional to $\exp(-0.0597854x/\sigma)$. The proportionality constant, which results from the initial condition, does not change the slope of the curves in Fig. 2 and is used as a fit parameter. As can be seen in Fig. 2, this prediction is in very good agreement with the simulation results even for strong gravitational fields. The same line of argument also allows one to obtain the form predicted by Eqs. (25) and (26) for $v_g/v_0 = 1/6$ and $v_g/v_0 = 1/24$, which are also plotted in Fig. 2 and which are also found to be in excellent agreement with the simulation results [and with the simpler theoretical result (20), which is reasonable in these cases]. The remaining deviation between theory and simulation for the case of strong fields is likely to be caused by effects from the wall, which is not included in the prediction from the two-field model.

B. Harmonic traps

We consider circular harmonic traps of the form (18) with adjustable trapping strength k and trap radius r_t . This form of a trap is popular in numerical studies on the collective behavior of ABPs in external force fields [36,84,86–89]. In experiments, such harmonic traps have already been realized by using optic [90] and acoustic [91,92] tweezers. Passive Brownian particles in such harmonic traps accumulate in the center. ABPs, on the other hand, can show many more effects: Their self-propulsion can overcome an attractive trap potential [86], they can confine passive particles inside a trap [36], and they can form active shells [86,93]. It has also been shown experimentally that active particles inside traps can be found in the center or at a certain distance from the center, depending on the propulsion speed of the particles and strength of the trap [87].

Here we focus on the accumulation of particles and the occurrence of MIPS in the traps. From Brownian dynamics simulations, we obtain the average number density ρ_{trap} inside the trap for various trapping strengths k and trap radii r_t . As an initial condition, we use a homogeneous packing density of $\Phi = 0.2$. For comparison, we consider also the phase behavior of the corresponding passive particles ($v_0 = 0$) and noninteracting ABPs. The occurrence of MIPS inside a harmonic trap requires that the density of active particles in the trap is sufficiently high. We predict the onset of MIPS by numerically determining when $D(\rho)$ in Eq. (16) becomes zero. This was achieved by numerically solving Eq. (12) for the case of harmonic traps and analyzing for which combinations of kr_t and r_t we get $D(\rho) = 0$. $D(\rho) = 0$ is the standard criterion for the spinodal for MIPS [58] and can be derived using a linear stability analysis [56]. The results are shown in Fig. 3.

As the trapping strength is (much) greater than the Brownian fluctuation strength for all traps except for the one where $k = 0$, the passive particles straightforwardly accumulate inside the trap [see Fig. 3(a)]. For a stronger or larger trap, the packing density of passive particles in the center of the trap

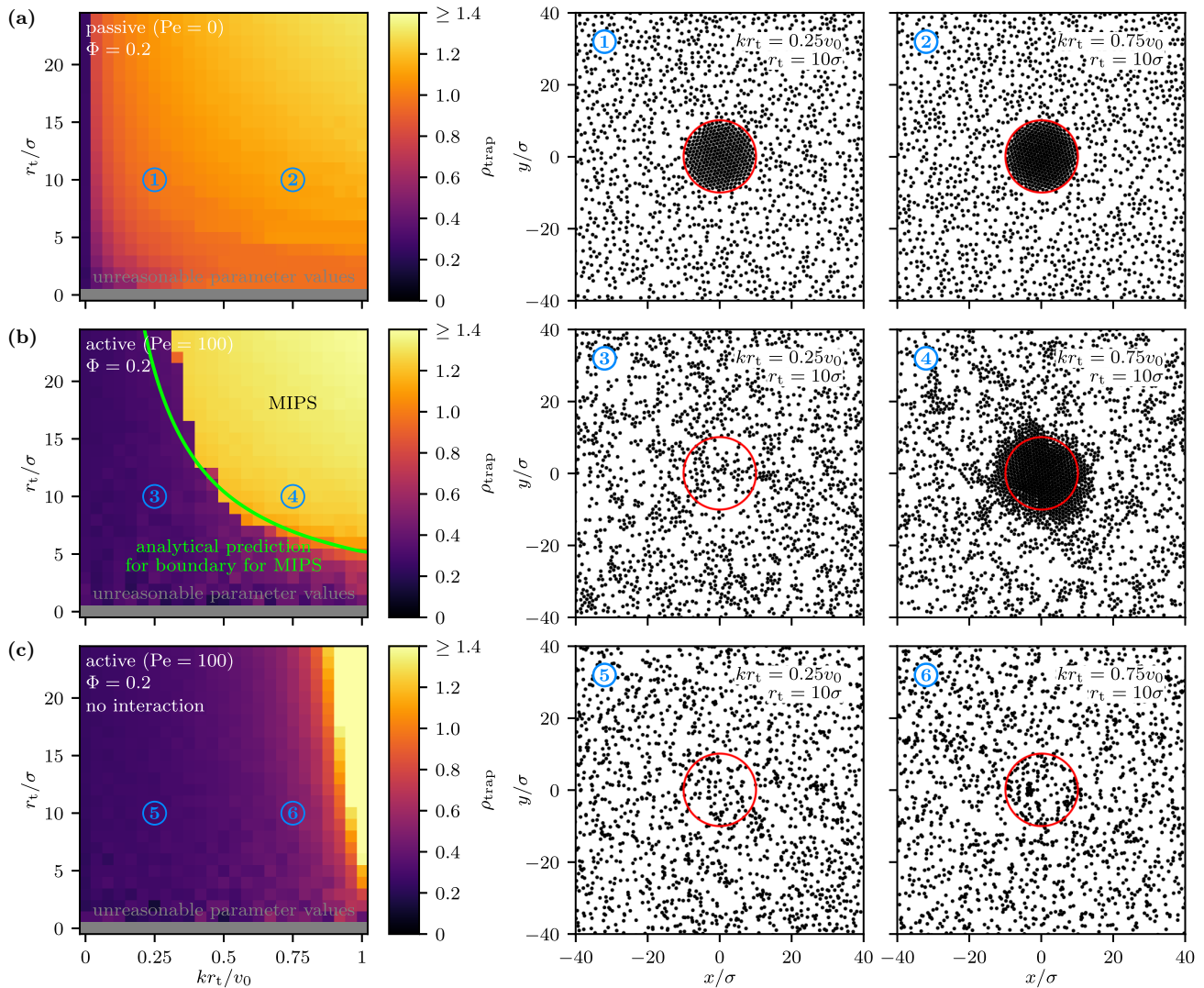


FIG. 3. Average number density ρ_{trap} inside a harmonic trap as a function of trapping strength k and trap radius r_t . (a) In the case of passive particles and a nonzero k , ρ_{trap} increases smoothly when k or r_t are increased. Respective snapshots show that passive particles always accumulate inside the trap. (b) In contrast, for active particles ρ_{trap} increases suddenly and sharply when entering a region of sufficiently large k and r_t where the ABPs undergo MIPS locally. Respective snapshots show that ABPs do not accumulate in a weak trap as their self-propulsion allows them to escape, whereas a strong trap allows for a MIPS cluster emerging inside the trap. Since ABPs accumulate at boundaries, the cluster formed in a trap can extend beyond the trap's boundary. (c) For noninteracting ABPs, no accumulation inside the trap can be observed, except for the case of very strong traps ($kr_t \approx 1$). However, for increasing kr_t , a gradual increase of ρ_{trap} can be observed as the ABPs stay longer inside the trap area. The bottom row of all state diagrams is shaded in gray because, for $r_t/\sigma = 0$, we necessarily have $kr_t/v_0 = 0$. See Ref. [80] for the raw data corresponding to this figure.

is larger [see snapshots 1 and 2 in Fig. 3(a)]. Therefore the average density inside the trap ρ_{trap} increases smoothly with the trapping strength k and trap radius r_t [see state diagram in Fig. 3(a)].

ABPs, on the other hand, behave quite differently [see Fig. 3(b)]. Due to their self-propulsion, they can escape from weak or small traps, resulting in a very low average density ρ_{trap} in the trap for small k or r_t . An example is a trap with parameters $kr_t = 0.25v_0$ and $r_t = 10\sigma$ [see snapshot 3 in Fig. 3(b)]. In this case no accumulation of ABPs is found, albeit passive particles would accumulate inside the same trap [cf. snapshot 1 in Fig. 3(a)]. When the trap becomes stronger and larger, the ABPs can remain inside the trap for a longer time and thus enhance the local concentration of

ABPs. If the local density inside the trap increases so far that it becomes larger than the critical density for the onset of MIPS [56,58,59], particle clustering emerges locally. Note that we chose the activity of the particles sufficiently large to allow for MIPS [67]. As the (local) MIPS clusters are tightly packed, ρ_{trap} suddenly increases when MIPS occurs [see state diagram in Fig. 3(b)]. Thus, since different physical mechanisms are in play due to the very different activities, it can be misleading to simply compare the right-hand sides of Figs. 3(a) and 3(b), since such a comparison could (due to the fact that the pictures look very similar) create the false impression that the differences are rather small.

Our analytical prediction for the onset of MIPS and the sudden increase of ρ_{trap} in the simulation data are in very

good agreement. They deviate only slightly for very large traps. We believe that this discrepancy originates from the fact that cluster formation inside a large trap significantly reduces the overall packing density around the trap, whereas our analytical approach assumes that density to be constant at $\Phi = 0.2$. Furthermore, the increase of ρ_{trap} that is associated with entering the MIPS region in the state diagram is less pronounced for very small but strong traps. This can be explained as follows: For a very small trap, the overall number of ABPs inside the trap is very small, which makes ρ_{trap} quite susceptible to Brownian fluctuations. While the accumulation of passive particles is restricted to the trap, ABPs can form clusters that extend beyond the boundary of the trap. This effect can be observed, e.g., for a trap with parameters $kr_t = 0.75v_0$ and $r_t = 10\sigma$ [see snapshot 4 in Fig. 3(b)], which corresponds to a point that is well inside the MIPS region in the state diagram. Moreover, the effect is closely related to the known phenomenon that ABPs accumulate at walls or other stationary obstacles [82,83], where the MIPS cluster inside the trap here acts as a fixed obstacle.

It is worth explaining here why we call the particle accumulation shown on the right-hand side of Fig. 3(b) “motility-induced phase separation,” even though it is clearly induced by the trap and remains, apart from a small crown, within the trap rather than having a size proportional to that of the system (as one would expect for phase separation and for MIPS in particular). Here it is worth pointing out that, despite its name, “motility-induced phase separation” is actually induced by a combination of three factors, namely, (i) motility, (ii) repulsive interactions, and (iii) a sufficiently high initial density. Active particles without repulsive interactions and interacting active particles whose overall concentration is extremely low will not show MIPS. In the scenario shown in Fig. 3(b), factors (i) and (ii) are always present (the particles are motile and interacting). Factor (iii)—an initial density that is sufficiently high to trigger the feedback mechanism leading to MIPS—is present only within the trap, which leads to a locally higher particle concentration and thus to the emergence of a local MIPS cluster. That the observed phase separation is indeed a form of MIPS is further confirmed by the fact that, as noted above and shown on the left-hand side of Fig. 3(b), the standard analytical criterion for MIPS [$D(\rho) = 0$] predicts the transition very accurately. Note that if the average density of the system is chosen within the binodal region for MIPS, the locally induced MIPS can become a global phase transition and, consequently, the MIPS clusters can outgrow the trap area.

To have a further test for the claim that we observe MIPS, we have performed additional simulations for a system of *noninteracting* ABPs in the same trap. The results are shown in Fig. 3(c). The state diagram on the left-hand side shows that a particle accumulation in the trap is observed only if the trap is very strong ($kr_t/v_0 \approx 1$). There is only a gradual increase of the density inside the trap when the trap strength is increased due to the fact that the particles spend, on average, more time inside the trap if it is stronger. In particular, as can be seen in the snapshots on the right-hand side of Fig. 3(c), there is no phase separation for the parameter values $kr_t = 0.75v_0$ and $r_t = 10\sigma$, for which there *is* phase separation in the interacting case. From this we can infer that the accumulation observed

on the right-hand side of Fig. 3(b) is not only due to the trap (if it were, it would also be observed in the noninteracting case) but also due to the interactions—as is characteristic for MIPS.

IV. CONCLUSIONS

We investigated the collective dynamics of ABPs under the influence of external force fields in 2D and 3D. For this purpose we derived predictive field theories from the Langevin equations that describe the motion of the ABPs on a microscopic level. These field theories are applicable for small to large densities and activities of the particles. In particular, the derived field theories are an advection-diffusion model, which contains up to two spatial derivatives per term and is the main focus of our current investigation, and a phase-field model, which contains derivatives up to fourth order. With the advection-diffusion model, we studied the effect of gravitation and harmonic traps on the steady state of the ABPs. For ABPs under gravity, we obtained a modified barometric density law that takes the interactions and activity of the particles into account. In the case of the harmonic traps, we predicted for which trap sizes and trapping forces the traps induce MIPS in the system. To confirm our predictions, we performed Brownian dynamics simulations. Their results were found to be in very good agreement with our analytical predictions. In summary, our results show that ABPs in external fields can exhibit interesting effects that arise from the coupling of the external force, the interactions of the particles, and their activity. An understanding of this coupling is helpful for future applications of ABPs [34,36], where external fields are likely to be relevant, and available through our field theories.

As, according to our results, the occurrence of MIPS can be controlled quite arbitrarily by external fields, such fields allow to realize programmable density patterns in systems containing ABPs. Since active particles are known to have a strong effect on the behavior of passive particles [77], it is likely that also programmable materials that contain both active and passive particles can be realized. In the future one should continue this study towards time-dependent external fields, for which our models are applicable as well if the fields do not change too fast with time. When extending our phase-field model by including terms up to sixth order in derivatives, one could use the extended model to study ABPs in high-gravity regions that can induce crystallization of the ABPs [94,95]. Furthermore, one could take external torques into account, which can result in a nematic ordering of the particles, allowing for interesting effects like floating phases [96,97].

ACKNOWLEDGMENTS

We thank S. Hartmann and U. Thiele for helpful discussions. R.W. is funded by the Deutsche Forschungsgemeinschaft (DFG, German Research Foundation) through Grant No. WI 4170/3-1. The simulations for this work were performed on the computer cluster PALMA II of the University of Münster.

APPENDIX A: DERIVATION DETAILS

Here we provide a brief introduction to the interaction-expansion method (IEM), which is used to derive the second-

and fourth-order-derivatives models from the Smoluchowski equation (6). A detailed review can be found in Ref. [57].

The IEM makes use of the BBGKY hierarchy [98]. This hierarchy arises when one derives a dynamic equation for the one-particle density field ϱ , defined by Eq. (7) for two spatial dimensions or (8) for three spatial dimensions, by integrating Eq. (6) over the degrees of freedom of particles all except for one. The resulting dynamic equation for ϱ involves a nonlocal term resulting from particle interactions which depends on the unknown two-particle density. For, e.g., two spatial dimensions, this term is given by

$$\mathcal{I}(\vec{r}, \phi, t) \propto \int_{\mathbb{R}^2} d^2r' \int_0^{2\pi} d\phi' U_2'(\|\vec{r} - \vec{r}'\|) \frac{\vec{r} - \vec{r}'}{\|\vec{r} - \vec{r}'\|} \times \varrho^{(2)}(\vec{r}, \vec{r}', \phi, \phi', t). \quad (\text{A1})$$

Here, $U_2'(r) = dU_2(r)/dr$ is a shorthand notation. Similarly, a dynamic equation for the two-particle density derived in this way would depend on the three-particle density and so on. To obtain a closed and solvable dynamic equation for ϱ , one requires a closure, i.e., a way to express the unknown two-particle density in terms of something that is known. Different derivation methods differ in how this closure is achieved. In DDFT, for example, one uses the adiabatic approximation, where the two-particle density is calculated from an equilibrium free energy functional [50]. For the purpose of describing MIPS, however, it is advantageous to use a closure method that does not rely on equilibrium approaches. In the IEM, the two-particle distribution is expressed via the pair-distribution function using Eq. (9). The pair-distribution function can be approximated in the way discussed in Sec. II A using known analytical representations [67,68,99]. This allows us to transform the interaction integral (A1) into a local integral by performing a gradient expansion around $\vec{r}' = \vec{0}$. The angular dependency is further eliminated by performing a Fourier expansion (in two spatial dimensions) or spherical harmonics expansion (in three spatial dimensions). These steps lead to a dynamic equation for the orientation-dependent particle-number density

$$\dot{\varrho}(\vec{r}, \hat{u}, t) + \Theta^{(Q)}(\vec{r}, \hat{u}, t) = 0, \quad (\text{A2})$$

where $\Theta^{(Q)}(\vec{r}, \hat{u}, t)$ is a quasicurrent. To obtain the dynamic equations for the order-parameter fields $\rho(\vec{r}, t)$, $\vec{P}(\vec{r}, t)$, and $\underline{Q}(\vec{r}, t)$, a Cartesian order-parameter expansion of $\varrho(\vec{r}, \hat{u}, t)$, given by Eq. (21), is performed. As a consequence, the dynamics of the system is now captured by the time evolution of the order-parameter fields ρ , \vec{P} , and \underline{Q} , which is given by

$$\dot{\rho} + \vec{\nabla} \cdot \vec{J}^{(\rho)} = 0, \quad \dot{\vec{P}} + \vec{\Theta}^{(P)} = \vec{0}, \quad \dot{\underline{Q}} + \underline{\Theta}^{(Q)} = \underline{0}, \quad (\text{A3})$$

with the current $\vec{J}^{(\rho)}$ for the (conserved) concentration field and the quasicurrents $\vec{\Theta}^{(P)}$ and $\underline{\Theta}^{(Q)}$ for the (nonconserved) polarization vector and nematic tensor, respectively. We can now exploit the fact that nonconserved quantities typically relax much faster than conserved ones and hence can be well approximated as fully relaxed on the timescale of the dynamics of the conserved order-parameter fields. This approximation is the QSA mentioned in Secs. II A and III A, which is given by the assumption that $\vec{\Theta}^{(P)} = \vec{0}$ and $\underline{\Theta}^{(Q)} = \underline{0}$ on the timescale of the concentration field. Note that this does

not imply that the higher-order order-parameter fields themselves become zero. The equations $\vec{\Theta}^{(P)} = \vec{0}$ and $\underline{\Theta}^{(Q)} = \underline{0}$, solved for \vec{P} and \underline{Q} , are constitutive equations for \vec{P} and \underline{Q} . These constitutive equations can then be recursively inserted into themselves and into $\vec{J}^{(\rho)}$. By truncating the gradient expansion at order n (e.g., $n = 2$ or $n = 4$), the constitutive equations for the higher-order order-parameter fields can be written in the form

$$\vec{P} = \vec{f}^{(P)}(\rho), \quad \underline{Q} = \underline{f}^{(Q)}(\rho), \quad (\text{A4})$$

with functions $\vec{f}^{(P)}$ and $\underline{f}^{(Q)}$. Thereby we have written \vec{P} and \underline{Q} in terms of the concentration field and its spatial derivatives. If we insert Eq. (A4) into $\vec{J}^{(\rho)}$, we obtain a closed dynamic equation for ρ alone. The contributions from polarization and nematic order are nevertheless taken into account in this dynamic equation—they have not been ignored, they are only expressed via ρ using Eq. (A4). This is important for the ability of field-theoretical models of this type to describe MIPS, where the mechanical equilibrium at the interface results from orientational contributions [100–102].

APPENDIX B: MICROSCOPIC EXPRESSIONS FOR THE COEFFICIENTS OCCURRING IN EQS. (13) AND (15)

The coefficients $\{a_i\}$ in Eq. (13) and $\{b_i\}$ in Eq. (15) can be related to microscopic properties of the system. In the following we present the corresponding expressions for 2D and 3D.

1. Two spatial dimensions

In 2D, the coefficients $\{a_i\}$ and $\{b_i\}$ are given by

$$a_0 = \frac{v_0^2}{2D_R}, \quad (\text{B1})$$

$$a_1 = \frac{A(1, 0, 0)}{\pi} - \frac{v_0}{\pi D_R} [2A(0, 1, 0) + A(0, 1, -1)], \quad (\text{B2})$$

$$a_2 = \frac{4}{\pi^2 D_R} A(0, 1, 0) [A(0, 1, 0) + A(0, 1, -1)], \quad (\text{B3})$$

$$b_1 = \frac{v_0^2}{2D_R^2}, \quad (\text{B4})$$

$$b_2 = -\frac{v_0}{\pi D_R^2} [A(0, 1, -1) + 3A(0, 1, 0)], \quad (\text{B5})$$

$$b_3 = \frac{4A(0, 1, 0)}{\pi^2 D_R^2} [A(0, 1, -1) + A(0, 1, 0)], \quad (\text{B6})$$

$$b_4 = -\frac{2v_0 A(0, 1, 0)}{\pi D_R^2}. \quad (\text{B7})$$

We follow the notation of Ref. [56], which gives approximate expressions for the coefficients $A(n, k_1, k_2)$ that originate from the pair-distribution function of the particles given in Ref. [67]. The coefficients occurring in Eqs. (B1)–(B7) are approximately given by [56,67]

$$A(1, 0, 0) = (38.2 + 18.4e^{2.87\Phi})\sigma^4 \tau_{LJ}^{-1}, \quad (\text{B8})$$

$$A(0, 1, 0) = 36.95\sigma^3 \tau_{LJ}^{-1}, \quad (\text{B9})$$

$$A(0, 1, -1) = -(0.23 + 13.6\Phi)\sigma^3 \tau_{LJ}^{-1}, \quad (\text{B10})$$

where the packing density Φ in 2D is related to the spatially averaged particle-number density $\bar{\rho}$ by $\Phi = \pi \bar{\rho} \sigma^2 / 4$ [56].

2. Three spatial dimensions

In 3D the coefficients $\{a_i\}$ and $\{b_i\}$ are given by

$$a_0 = \frac{v_0^2}{6D_R}, \quad (\text{B11})$$

$$a_1 = \frac{2G(1, 0, 0, 0)}{3\pi} - \frac{v_0}{3\pi D_R} [3G(0, 1, 1, 0) + G(0, 1, 0, 1)], \quad (\text{B12})$$

$$a_2 = \frac{4}{3\pi^2 D_R} G(0, 1, 1, 0) [G(0, 1, 1, 0) + G(0, 1, 0, 1)], \quad (\text{B13})$$

$$b_1 = \frac{v_0^2}{12D_R^2}, \quad (\text{B14})$$

$$b_2 = -\frac{v_0}{6\pi D_R^2} [G(0, 1, 0, 1) + 3G(0, 1, 1, 0)], \quad (\text{B15})$$

$$b_3 = \frac{2G(0, 1, 1, 0)}{3\pi^2 D_R^2} [G(0, 1, 0, 1) + G(0, 1, 1, 0)], \quad (\text{B16})$$

$$b_4 = -\frac{v_0 G(0, 1, 1, 0)}{3\pi D_R^2}. \quad (\text{B17})$$

Here we use the notation of Ref. [60] for the coefficients $G(n, l_1, l_2, l_3)$ originating from the pair-distribution function given in Ref. [68]. The coefficients occurring in Eqs. (B11)–(B17) are approximately given by

$$G(1, 0, 0, 0) = (41.59 + 12.69e^{4.07\Phi})\sigma^5\tau_{LJ}^{-1}, \quad (\text{B18})$$

$$G(0, 1, 1, 0) = (22.49 + 7.05\Phi)\sigma^4\tau_{LJ}^{-1}, \quad (\text{B19})$$

$$G(0, 1, 0, 1) = -20.48\sigma^4\tau_{LJ}^{-1}, \quad (\text{B20})$$

where Φ denotes the overall packing density in 3D that is related to the spatially averaged particle-number density $\bar{\rho}$ by $\Phi = \pi \bar{\rho} \sigma^3 / 6$ [60,68].

-
- [1] J. Elgeti, R. G. Winkler, and G. Gompper, Physics of microswimmers—Single particle motion and collective behavior: A review, *Rep. Prog. Phys.* **78**, 056601 (2015).
- [2] T. Speck, Collective behavior of active Brownian particles: From microscopic clustering to macroscopic phase separation, *Eur. Phys. J. Spec. Top.* **225**, 2287 (2016).
- [3] A. Zöttl and H. Stark, Emergent behavior in active colloids, *J. Phys.: Condens. Matter* **28**, 253001 (2016).
- [4] C. Bechinger, R. Di Leonardo, H. Löwen, C. Reichardt, G. Volpe, and G. Volpe, Active particles in complex and crowded environments, *Rev. Mod. Phys.* **88**, 045006 (2016).
- [5] J. Katuri, K. D. Seo, D. S. Kim, and S. Sanchez, Artificial micro-swimmers in simulated natural environments, *Lab Chip* **16**, 1101 (2016).
- [6] H. Stark, Swimming in external fields, *Eur. Phys. J. Spec. Top.* **225**, 2369 (2016).
- [7] Z. Wang, H.-Y. Chen, Y.-J. Sheng, and H.-K. Tsao, Diffusion, sedimentation equilibrium, and harmonic trapping of run-and-tumble nanoswimmers, *Soft Matter* **10**, 3209 (2014).
- [8] F. Ginot, I. Theurkauff, D. Levis, C. Ybert, L. Bocquet, L. Berthier, and C. Cottin-Bizonne, Nonequilibrium equation of state in suspensions of active colloids, *Phys. Rev. X* **5**, 011004 (2015).
- [9] J. Vachier and M. G. Mazza, Dynamics of sedimenting active Brownian particles, *Eur. Phys. J. E* **42**, 11 (2019).
- [10] A. I. Campbell and S. J. Ebbens, Gravitaxis in spherical Janus swimming devices, *Langmuir* **29**, 14066 (2013).
- [11] K. Wolff, A. M. Hahn, and H. Stark, Sedimentation and polar order of active bottom-heavy particles, *Eur. Phys. J. E* **36**, 43 (2013).
- [12] E. Locatelli, F. Baldovin, E. Orlandini, and M. Pierno, Active Brownian particles escaping a channel in single file, *Phys. Rev. E* **91**, 022109 (2015).
- [13] A. I. Campbell, R. Wittkowski, B. ten Hagen, H. Löwen, and S. J. Ebbens, Helical paths, gravitaxis, and separation phenomena for mass-anisotropic self-propelling colloids: Experiment versus theory, *J. Chem. Phys.* **147**, 084905 (2017).
- [14] F. Ginot, A. Solon, Y. Kafri, C. Ybert, J. Tailleur, and C. Cottin-Bizonne, Sedimentation of self-propelled Janus colloids: Polarization and pressure, *New J. Phys.* **20**, 115001 (2018).
- [15] B. ten Hagen, F. Kümmel, R. Wittkowski, D. Takagi, H. Löwen, and C. Bechinger, Gravitaxis of asymmetric self-propelled colloidal particles, *Nat. Commun.* **5**, 4829 (2014).
- [16] J. Tailleur and M. E. Cates, Sedimentation, trapping, and rectification of dilute bacteria, *EPL* **86**, 60002 (2009).
- [17] A. Pototsky and H. Stark, Active Brownian particles in two-dimensional traps, *EPL* **98**, 50004 (2012).
- [18] H. M. López, J. Gachelin, C. Douarche, H. Auradou, and E. Clément, Turning bacteria suspensions into superfluids, *Phys. Rev. Lett.* **115**, 028301 (2015).
- [19] S. C. Takatori and J. F. Brady, Superfluid behavior of active suspensions from diffusive stretching, *Phys. Rev. Lett.* **118**, 018003 (2017).
- [20] J. Palacci, C. Cottin-Bizonne, C. Ybert, and L. Bocquet, Sedimentation and effective temperature of active colloidal suspensions, *Phys. Rev. Lett.* **105**, 088304 (2010).
- [21] C. Maggi, A. Lepore, J. Solari, A. Rizzo, and R. Di Leonardo, Motility fractionation of bacteria by centrifugation, *Soft Matter* **9**, 10885 (2013).
- [22] N. Koumakis, C. Maggi, and R. Di Leonardo, Directed transport of active particles over asymmetric energy barriers, *Soft Matter* **10**, 5695 (2014).
- [23] S. Hermann and M. Schmidt, Active ideal sedimentation: Exact two-dimensional steady states, *Soft Matter* **14**, 1614 (2018).
- [24] M. Hennes, K. Wolff, and H. Stark, Self-induced polar order of active Brownian particles in a harmonic trap, *Phys. Rev. Lett.* **112**, 238104 (2014).

- [25] J. Elgeti and G. Gompper, Wall accumulation of self-propelled spheres, *EPL* **101**, 48003 (2013).
- [26] C. F. Lee, Active particles under confinement: Aggregation at the wall and gradient formation inside a channel, *New J. Phys.* **15**, 055007 (2013).
- [27] E. Mones, A. Czirók, and T. Vicsek, Anomalous segregation dynamics of self-propelled particles, *New J. Phys.* **17**, 063013 (2015).
- [28] A. P. Solon, Y. Fily, A. Baskaran, M. E. Cates, Y. Kafri, M. Kardar, and J. Tailleur, Pressure is not a state function for generic active fluids, *Nat. Phys.* **11**, 673 (2015).
- [29] A. P. Solon, J. Stenhammar, M. E. Cates, Y. Kafri, and J. Tailleur, Generalized thermodynamics of motility-induced phase separation: Phase equilibria, Laplace pressure, and change of ensembles, *New J. Phys.* **20**, 075001 (2018).
- [30] N. Koumakis, A. Lepore, C. Maggi, and R. Di Leonardo, Targeted delivery of colloids by swimming bacteria, *Nat. Commun.* **4**, 2588 (2013).
- [31] X. Ma, K. Hahn, and S. Sanchez, Catalytic mesoporous Janus nanomotors for active cargo delivery, *J. Am. Chem. Soc.* **137**, 4976 (2015).
- [32] J. Li, B. E.-F. de Ávila, W. Gao, L. Zhang, and J. Wang, Micro/Nanorobots for biomedicine: Delivery, surgery, sensing, and detoxification, *Sci. Rob.* **2**, eaam6431 (2017).
- [33] I. Santiago, Nanoscale active matter matters: Challenges and opportunities for self-propelled nanomotors, *Nano Today* **19**, 11 (2018).
- [34] T. Nitschke, J. Stenhammar, and R. Wittkowski, Collective guiding of acoustically propelled nano- and microparticles, *Nanoscale Adv.* **4**, 2844 (2022).
- [35] *Active Materials*, edited by P. Fratzl, M. Friedman, K. Krauthausen, and W. Schäffner, De Gruyter STEM (De Gruyter, Berlin, 2021).
- [36] W. Yang, V. R. Misko, F. Marchesoni, and F. Nori, Colloidal transport through trap arrays controlled by active microswimmers, *J. Phys.: Condens. Matter* **30**, 264004 (2018).
- [37] K. J. Rao, F. Li, L. Meng, H. Zheng, F. Cai, and W. Wang, A force to be reckoned with: A review of synthetic microswimmers powered by ultrasound, *Small* **11**, 2836 (2015).
- [38] Z. Wu, X. Lin, T. Si, and Q. He, Recent progress on bioinspired self-propelled micro/nanomotors via controlled molecular self-assembly, *Small* **12**, 3080 (2016).
- [39] T. Xu, W. Gao, L.-P. Xu, X. Zhang, and S. Wang, Fuel-free synthetic micro-/nanomachines, *Adv. Mater.* **29**, 1603250 (2017).
- [40] M. Guix, S. M. Weiz, O. G. Schmidt, and M. Medina-Sánchez, Self-propelled micro/nanoparticle motors, *Part. Part. Syst. Char.* **35**, 1700382 (2018).
- [41] X. Chang, C. Chen, J. Li, X. Lu, Y. Liang, D. Zhou, H. Wang, G. Zhang, T. Li, J. Wang *et al.*, Motile micropump based on synthetic micromotors for dynamic micropatterning, *ACS Appl. Mater. Interfaces* **11**, 28507 (2019).
- [42] M. Pacheco-Jerez and B. Jurado-Sánchez, Biomimetic nanoparticles and self-propelled micromotors for biomedical applications, in *Materials for Biomedical Engineering*, edited by A.-M. Holban and A. M. Grumezescu (Elsevier, Amsterdam, 2019), pp. 1–31.
- [43] J. Schwarz-Linek, J. Arlt, A. Jepsen, A. Dawson, T. Vissers, D. Miroti, T. Pilizota, V. A. Martinez, and W. C. Poon, *Escherichia coli* as a model active colloid: A practical introduction, *Colloids Surf. B* **137**, 2 (2016).
- [44] C. Chen, S. Liu, X. Shi, H. Chaté, and Y. Wu, Weak synchronization and large-scale collective oscillation in dense bacterial suspensions, *Nature* **542**, 210 (2017).
- [45] T. Andac, P. Weigmann, S. K. P. Velu, E. Pinçe, G. Volpe, G. Volpe, and A. Callegari, Active matter alters the growth dynamics of coffee rings, *Soft Matter* **15**, 1488 (2019).
- [46] J. Tailleur and M. E. Cates, Statistical mechanics of interacting run-and-tumble bacteria, *Phys. Rev. Lett.* **100**, 218103 (2008).
- [47] M. E. Cates and J. Tailleur, When are active Brownian particles and run-and-tumble particles equivalent? Consequences for motility-induced phase separation, *EPL* **101**, 20010 (2013).
- [48] G. Liu, A. Patch, F. Bahar, D. Yllanes, R. D. Welch, M. C. Marchetti, S. Thutupalli, and J. W. Shaevitz, Self-driven phase transitions drive *Myxococcus xanthus* fruiting body formation, *Phys. Rev. Lett.* **122**, 248102 (2019).
- [49] C. G. Wagner, M. F. Hagan, and A. Baskaran, Steady-state distributions of ideal active Brownian particles under confinement and forcing, *J. Stat. Mech.: Theory Exp.* (2017) 043203.
- [50] M. te Vrugt, H. Löwen, and R. Wittkowski, Classical dynamical density functional theory: From fundamentals to applications, *Adv. Phys.* **69**, 121 (2020).
- [51] A. M. Menzel, A. Saha, C. Hoell, and H. Löwen, Dynamical density functional theory for microswimmers, *J. Chem. Phys.* **144**, 024115 (2016).
- [52] C. Hoell, H. Löwen, and A. M. Menzel, Dynamical density functional theory for circle swimmers, *New J. Phys.* **19**, 125004 (2017).
- [53] C. Hoell, H. Löwen, and A. M. Menzel, Multi-species dynamical density functional theory for microswimmers: Derivation, orientational ordering, trapping potentials, and shear cells, *J. Chem. Phys.* **151**, 064902 (2019).
- [54] U. M. B. Marconi and C. Maggi, Towards a statistical mechanical theory of active fluids, *Soft Matter* **11**, 8768 (2015).
- [55] P. Jung and P. Hänggi, Dynamical systems: A unified colored-noise approximation, *Phys. Rev. A* **35**, 4464 (1987).
- [56] J. Bickmann and R. Wittkowski, Predictive local field theory for interacting active Brownian spheres in two spatial dimensions, *J. Phys.: Condens. Matter* **32**, 214001 (2020).
- [57] M. te Vrugt, J. Bickmann, and R. Wittkowski, How to derive a predictive field theory for active Brownian particles: A step-by-step tutorial, *J. Phys.: Condens. Matter* **35**, 313001 (2023).
- [58] M. E. Cates and J. Tailleur, Motility-induced phase separation, *Annu. Rev. Condens. Matter Phys.* **6**, 219 (2015).
- [59] R. Wittkowski, J. Stenhammar, and M. E. Cates, Nonequilibrium dynamics of mixtures of active and passive colloidal particles, *New J. Phys.* **19**, 105003 (2017).
- [60] J. Bickmann and R. Wittkowski, Collective dynamics of active Brownian particles in three spatial dimensions: A predictive field theory, *Phys. Rev. Res.* **2**, 033241 (2020).
- [61] J. Bickmann, S. Bröker, J. Jeggle, and R. Wittkowski, Analytical approach to chiral active systems: Suppressed phase separation of interacting Brownian circle swimmers, *J. Chem. Phys.* **156**, 194904 (2022).

- [62] M. te Vrugt, T. Frohoff-Hülsmann, E. Heifetz, U. Thiele, and R. Wittkowski, From a microscopic inertial active matter model to the Schrödinger equation, *Nat. Commun.* **14**, 1302 (2023).
- [63] A. J. M. Yang, P. D. Fleming, and J. H. Gibbs, Molecular theory of surface tension, *J. Chem. Phys.* **64**, 3732 (1976).
- [64] R. Evans, The nature of the liquid-vapour interface and other topics in the statistical mechanics of non-uniform, classical fluids, *Adv. Phys.* **28**, 143 (1979).
- [65] H. Emmerich, H. Löwen, R. Wittkowski, T. Gruhn, G. I. Tóth, G. Tegze, and L. Gránásy, Phase-field-crystal models for condensed matter dynamics on atomic length and diffusive time scales: An overview, *Adv. Phys.* **61**, 665 (2012).
- [66] M. te Vrugt and R. Wittkowski, Relations between angular and Cartesian orientational expansions, *AIP Adv.* **10**, 035106 (2020).
- [67] J. Jeggle, J. Stenhammar, and R. Wittkowski, Pair-distribution function of active Brownian spheres in two spatial dimensions: Simulation results and analytic representation, *J. Chem. Phys.* **152**, 194903 (2020).
- [68] S. Bröker, M. te Vrugt, J. Jeggle, J. Stenhammar, and R. Wittkowski, Pair-distribution function of active Brownian spheres in three spatial dimensions: Simulation results and analytical representation, [arXiv:2307.14558](https://arxiv.org/abs/2307.14558).
- [69] R. Wittkowski, A. Tiribocchi, J. Stenhammar, R. J. Allen, D. Marenduzzo, and M. E. Cates, Scalar ϕ^4 field theory for active-particle phase separation, *Nat. Commun.* **5**, 4351 (2014).
- [70] E. Tjhung, C. Nardini, and M. E. Cates, Cluster phases and bubbly phase separation in active fluids: Reversal of the Ostwald process, *Phys. Rev. X* **8**, 031080 (2018).
- [71] See Supplemental Material at <http://link.aps.org/supplemental/10.1103/PhysRevE.108.044601> for microscopic expressions for the expansion coefficients appearing in the density current.
- [72] J. Bialké, H. Löwen, and T. Speck, Microscopic theory for the phase separation of self-propelled repulsive disks, *EPL* **103**, 30008 (2013).
- [73] Wolfram Research Inc., Mathematica, Version 12.1 (2020), Champaign, Illinois, USA.
- [74] S. Plimpton, Fast parallel algorithms for short-range molecular dynamics, *J. Comput. Phys.* **117**, 1 (1995).
- [75] J. D. Weeks, D. Chandler, and H. C. Andersen, Role of repulsive forces in determining the equilibrium structure of simple liquids, *J. Chem. Phys.* **54**, 5237 (1971).
- [76] J. Stenhammar, D. Marenduzzo, R. J. Allen, and M. E. Cates, Phase behaviour of active Brownian particles: The role of dimensionality, *Soft Matter* **10**, 1489 (2014).
- [77] J. Stenhammar, R. Wittkowski, D. Marenduzzo, and M. E. Cates, Activity-induced phase separation and self-assembly in mixtures of active and passive particles, *Phys. Rev. Lett.* **114**, 018301 (2015).
- [78] A. P. Solon, J. Stenhammar, R. Wittkowski, M. Kardar, Y. Kafri, M. E. Cates, and J. Tailleur, Pressure and phase equilibria in interacting active Brownian spheres, *Phys. Rev. Lett.* **114**, 198301 (2015).
- [79] J. Stenhammar, R. Wittkowski, D. Marenduzzo, and M. E. Cates, Light-induced self-assembly of active rectification devices, *Sci. Adv.* **2**, e1501850 (2016).
- [80] See <https://doi.org/10.5281/zenodo.5957520> for the raw data underlying this study.
- [81] T. F. F. Farage, P. Krinninger, and J. M. Brader, Effective interactions in active Brownian suspensions, *Phys. Rev. E* **91**, 042310 (2015).
- [82] I. D. Vladescu, E. J. Marsden, J. Schwarz-Linek, V. A. Martinez, J. Arlt, A. N. Morozov, D. Marenduzzo, M. E. Cates, and W. C. K. Poon, Filling an emulsion drop with motile bacteria, *Phys. Rev. Lett.* **113**, 268101 (2014).
- [83] X. Yang, M. L. Manning, and M. C. Marchetti, Aggregation and segregation of confined active particles, *Soft Matter* **10**, 6477 (2014).
- [84] L. Caprini, E. Hernández-García, C. López, and U. M. B. Marconi, A comparative study between two models of active cluster crystals, *Sci. Rep.* **9**, 16687 (2019).
- [85] M. te Vrugt and R. Wittkowski, Orientational order parameters for arbitrary quantum systems, *Ann. Phys. (Berlin)* **532**, 2000266 (2020).
- [86] W. Yang, V. R. Misko, J. Tempere, M. Kong, and F. M. Peeters, Artificial living crystals in confined environment, *Phys. Rev. E* **95**, 062602 (2017).
- [87] C. Shen, L. Li, Z. Jiang, and H. D. Ou-Yang, Spatial and temporal fluctuation of an ABP in an optical trap, [arXiv:1908.08157](https://arxiv.org/abs/1908.08157).
- [88] H. E. Ribeiro, W. P. Ferreira, and F. Q. Potiguar, Trapping and sorting of active matter in a periodic background potential, *Phys. Rev. E* **101**, 032126 (2020).
- [89] L. Caprini, A. R. Sprenger, H. Löwen, and R. Wittmann, The parental active model: A unifying stochastic description of self-propulsion, *J. Chem. Phys.* **156**, 071102 (2022).
- [90] Z. Xu, W. Song, and K. B. Crozier, Optical trapping of nanoparticles using all-silicon nanoantennas, *ACS Photonics* **5**, 4993 (2018).
- [91] J. Lee, S.-Y. Teh, A. Lee, H. H. Kim, C. Lee, and K. K. Shung, Transverse acoustic trapping using a Gaussian focused ultrasound, *Ultrasound Med. Biol.* **36**, 350 (2010).
- [92] S. C. Takatori, R. de Dier, J. Vermant, and J. F. Brady, Acoustic trapping of active matter, *Nat. Commun.* **7**, 10694 (2016).
- [93] M. Sandoval, J. C. Hidalgo-Gonzalez, and J. I. Jimenez-Aquino, Self-driven particles in linear flows and trapped in a harmonic potential, *Phys. Rev. E* **97**, 032603 (2018).
- [94] J. F. Löffler and W. L. Johnson, Crystallization of Mg-Al and Al-based metallic liquids under ultra-high gravity, *Intermetallics* **10**, 1167 (2002).
- [95] X. He, Z. Wang, Y. Pu, D. Wang, R. Tang, S. Cui, J.-X. Wang, and J.-F. Chen, High-gravity-assisted scalable synthesis of zirconia nanodispersion for light emitting diodes encapsulation with enhanced light extraction efficiency, *Chem. Eng. Sci.* **195**, 1 (2019).
- [96] M. Schmidt, M. Dijkstra, and J.-P. Hansen, Floating liquid phase in sedimenting colloid-polymer mixtures, *Phys. Rev. Lett.* **93**, 088303 (2004).
- [97] D. de las Heras, N. Doshi, T. Cosgrove, J. Phipps, D. I. Gittins, J. S. van Duijneveldt, and M. Schmidt, Floating nematic phase in colloidal platelet-sphere mixtures, *Sci. Rep.* **2**, 789 (2012).
- [98] J.-P. Hansen and I. R. McDonald, *Theory of Simple Liquids*, 3rd ed. (Elsevier Academic Press, Amsterdam, 2006).
- [99] S. Bröker, M. te Vrugt, and R. Wittkowski, Collective dynamics and pair-distribution function of active Brownian ellipsoids, [arXiv:2307.15535](https://arxiv.org/abs/2307.15535).

- [100] C. F. Lee, Interface stability, interface fluctuations, and the Gibbs–Thomson relationship in motility-induced phase separations, *Soft Matter* **13**, 376 (2017).
- [101] A. K. Omar, Z.-G. Wang, and J. F. Brady, Microscopic origins of the swim pressure and the anomalous surface tension of active matter, *Phys. Rev. E* **101**, 012604 (2020).
- [102] N. Lauersdorf, T. Kolb, M. Moradi, E. Nazockdast, and D. Klotsa, Phase behavior and surface tension of soft active Brownian particles, *Soft Matter* **17**, 6337 (2021).